Change Detection Analysis of Humans Moving Behind Walls

MOENESS G. AMIN, Fellow, IEEE
FAUZIA AHMAD, Senior Member, IEEE
Villanova University

In this paper, we consider the problem of detection of humans behind walls and inside enclosed structures using radars. We use change detection techniques to mitigate the heavy clutter caused by strong reflections from exterior and interior walls. To improve spatial resolution, we apply multiple-input multiple-output (MIMO) configurations to moving target indication (MTI). We examine change detection formulation and performance when clutter removal is performed pre- and postbeamforming. Using signal multiplexing from two transmitters and several receiver positions, we show that the virtual array (coarray) implementing the prebeamforming change detection MIMO scheme permits enhanced clutter rejection and improvement in imaging resolution of moving targets without increasing the physical aperture. Laboratory experiments are conducted to validate the proposed approaches with targets walking behind walls.

I. INTRODUCTION

Detection of humans is one of the most important objectives in urban sensing and through-the-wall radar technology [1–7]. Humans belong to the class of animate objects that are characterized by motion of the limbs, breathing, and heartbeat. These features separate animate and inanimate objects and allow the detection of targets of interest to proceed based on changes in the phase of the scattered radar signals over successive probing and data observations.

Commonly applied techniques for the mitigation of electromagnetic (EM) reflections from the front wall when considering stationary targets are, namely, background subtraction [1], spatial filtering [8], wall subspace projections [9], and wall parameter estimation, modeling of wall returns, and subtraction of the modeled data from the total received signals [10]. The first approach of background subtraction achieves the best results and effectively removes all wall returns and nontarget clutter. The background or reference scene may not, however, be available for nonsurveillance modes of operation in which a relatively short period of time is allowed for image acquisition, processing, and interpretation. In the case of moving targets, the previously imaged scene can be considered as the background scene. In this case, the subtraction of two consecutive or nonconsecutive data frames or images yields performance similar to the background subtraction process for the case of stationary targets. The subtraction operation performed for either case of stationary or moving targets is referred to as change detection (CD). The length of the time period elapsing between the two data sets to be subtracted may differ for the two cases. While the stationary scene permits long time periods, the moving target case necessitates short periods. When operating on data frames, both operations can be described by what is known as delay line cancellers (DLCs) [11].

Moving target indication (MTI) processing applies clutter filters to remove radar returns scattered from stationary objects. DLCs can be designed such that their frequency responses place a notch at DC and concurrently meet other desirable passband and stopband filter characteristics [11]. Doppler filter banks typically follow the DLC and provide benefits of signal separations, radial velocity measurements, and noise reduction [11]. For urban sensing environments, changes in the backscattered signal phase due to motion do not necessarily lend themselves to Doppler frequency shifts. The human motion can be abrupt and highly nonstationary, producing a time-dependent phase whose rate of change may fail to translate into a single shift or multicomponent sinusoids that can be captured by different Doppler filters. Instead, the corresponding wide spectrum of human motions becomes nonlocalizable and can span the entire

radar frequency band. In lieu of Doppler filters, time-frequency processing can be applied to reveal the instantaneous frequency signatures, as it is the case with the human gait [12, 13, 14]. However, apart from regularized motions, such as walking and running, time-frequency Doppler signal representations are very complex and difficult to measure and interpret, especially when dealing with nonhomogeneous walls. Therefore, the application of Doppler and micro-Doppler filters for indoor target surveillance may not significantly add to target motion detection that is already achieved by DLCs.

In this paper, we consider CD combined with the benefits of high spatial resolution provided by multiple-input multiple-output (MIMO) configuration. CD in through-the-wall radar imaging (TWRI) was first discussed concurrently in [15] and [16]. In [15], the synchronous impulse reconstruction (SIRE) radar system, operating in the frequency band of 300 MHz–3 GHz and employing a multitransmit/receive design, was used for MTI. The CD approach discussed in [15] subtracts the downrange profiles over consecutive data frames, emulating a derivative operator. It was shown that the SIRE successfully detects a human target moving within an enclosed structure. On the other hand, CD was applied in [16] in the context of background subtraction to detect stationary targets using data acquired during interrogations of a scene at two different time instants. Image intensity subtraction was employed, and examples based on ray tracing data covering the 0.7 to 3.1-GHz frequency range were provided. More recently, [17] applied CD for slow-moving target detection in TWRI by subtracting the image intensity corresponding to different data frames, followed by a zero threshold operation to suppress the reference image. Examples of target detection in [17] included both EM modeling data and real experiments. CD using first- and second-order motion detection images for TWRI application were discussed in [18], [19]. The former has better sensitivity to motion, whereas the latter provides better signal-to-noise ratio. Experimental data, reported in [18], [19] using four antennas and a signal bandwidth of 500 MHz to 1 GHz, demonstrated that CD techniques are capable of detecting walking human and simulated human breathing using machine motion. Moving target indicator filtering was also used in [20] for detection of humans in motion inside buildings. An ultrawideband frequency-modulated continuous-wave (CW) radar with an extended frequency sweep from 0.5 to 8 GHz was used in the differential mode to track human motion behind a brick wall.

All of the aforementioned works focused on specific cases of CD, and none of them examined MIMO configurations in CD. MIMO radar-based CD for through-the-wall applications was first applied

in [21], followed soon after by [22]. However, no comprehensive analytical treatment of the MIMO CD was provided. In this paper, we focus on CD in both single-input multiple-output (SIMO) and MIMO imaging systems, aiming at detection of animate objects. We provide an in-depth analyses of both coherent and intensity CD schemes. Further, we provide insights into the effects of MIMO array layouts and signaling schemes on system performance. In particular, collocated configurations are considered wherein the transmitters and receivers are implemented on the same platform. The goal is to detect the presence of humans in the scene via a change of the backscatter phase over successive measurements. Rather than operating on successive pulses, DLC equivalences are applied to different data frames for each range bin (prebeamforming CD) or different images for each pixel (postbeamforming CD). The frames can be consecutive, dealing with targets exhibiting sudden short motions, or nonconsecutive with relatively long time difference, for the case in which the target changes its range gate position. Compared with a SIMO system, the MIMO radar yields an extended equivalent virtual array, or coarray, resulting in improved cross-range resolution of the moving target [23–26]. Improved resolution permits better localization of the targets. Real data collected in a laboratory environment is used to validate the proposed pre- and postbeamforming CD approaches and to compare the performance of the SIMO and MIMO systems. For consecutive frames, the prebeamforming CD has better performance than the postbeamforming CD. On the other hand, for nonconsecutive frames with the targets undergoing large displacements, both CD schemes are able to detect the targets; the prebeamforming CD scheme shows two sets of imaged targets corresponding to the target positions at the two data acquisitions, whereas the postbeamforming CD, due to zero thresholding, retains only one set of imaged targets, though with significantly more artifacts.

The paper is organized as follows. We describe the wideband MIMO radar configuration in Section II. Section III presents the signal model and the CD algorithms. Experimental setup and supporting results are provided in Section IV. Section V contains the conclusions.

II. WIDEBAND MIMO RADAR

Consider a MIMO radar with an M-element linear transmit array and an N-element linear receive array. Under narrowband far-field operation, the performance of a MIMO radar system is characterized by a virtual array or coarray [24, 25]. More specifically, let $f_m(t)$ denote the narrowband baseband signal transmitted by the mth transmit element with the phase center at $\mathbf{x}_{tm} = (x_{tm}, 0)$. Consider a
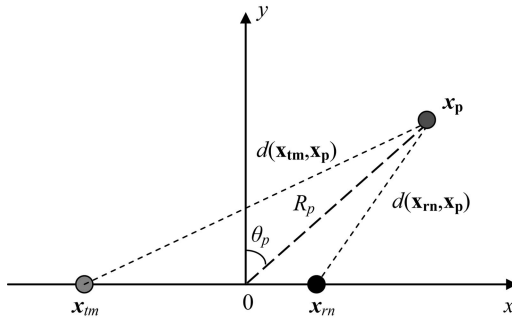
Fig. 1. Scene geometry.

single-point target located at range R_p in direction θ_p, as shown in Fig. 1. Then, the baseband signal $r_n(t)$ received by the nth receive element with the phase center at $\mathbf{x}_{rn} = (x_{rn}, 0)$ from the target at $\mathbf{x}_p = (x_p, y_p) = (R_p \sin\theta_p, R_p \cos\theta_p)$ is given by

$$r_n(t) = \sum_{m=0}^{M-1} \sigma_p f_m(t) \exp\{-j\omega_c \tau_{p,mn}\}, \qquad n = 0, 1, \ldots, N-1 \tag{1}$$

where σ_p is the complex reflectivity of the target, ω_c is the carrier frequency, and $\tau_{p,mn}$ is the propagation delay encountered by the signal as it travels from the mth transmitter to the target and then back to the nth receiver. As shown in Fig. 1, $\tau_{p,mn}$ is given by

$$\tau_{p,mn} = \frac{d(\mathbf{x}_{tm}, \mathbf{x}_p) + d(\mathbf{x}_{rn}, \mathbf{x}_p)}{c}. \tag{2}$$

In (2), $d(\cdot, \cdot)$ is the Cartesian distance between two position vectors, and c is the propagation speed. The distances $d(\mathbf{x}_{tm}, \mathbf{x}_p)$ and $d(\mathbf{x}_{rn}, \mathbf{x}_p)$ are given by

$$d(\mathbf{x}_{tm}, \mathbf{x}_p) = \sqrt{(x_{tm} - R_p \sin\theta_p)^2 + (R_p \cos\theta_p)^2}$$

$$= R_p \left(1 + \frac{x_{tm}^2}{R_p^2} - \frac{2x_{tm}\sin\theta_p}{R_p}\right)^{1/2}$$

$$d(\mathbf{x}_{rn}, \mathbf{x}_p) = \sqrt{(x_{rn} - R_p \sin\theta_p)^2 + (R_p \cos\theta_p)^2}$$

$$= R_p \left(1 + \frac{x_{rn}^2}{R_p^2} - \frac{2x_{rn}\sin\theta_p}{R_p}\right)^{1/2}. \tag{3}$$

Under far-field conditions, the range R_p is such that $x_{rn}/R_p \ll 1$, $x_{tm}/R_p \ll 1$ for all m, n. Accordingly, using the binomial theorem and retaining only the first-order powers of x_{rn}/R_p and x_{tm}/R_p, (3) can be rewritten as

$$d(\mathbf{x}_{tm}, \mathbf{x}_p) \approx R_p - x_{tm}\sin\theta_p$$
$$d(\mathbf{x}_{rn}, \mathbf{x}_p) \approx R_p - x_{rn}\sin\theta_p. \tag{4}$$

Therefore, for far-field propagation, the delay $\tau_{p,mn}$ takes the form

$$\tau_{p,mn} = \frac{2R_p - (x_{tm} + x_{rn})\sin\theta_p}{c}. \tag{5}$$

The delay factor $2R_p/c$ due to range is fixed for a given range cell and is thus ignored in the remainder of this section. Substituting (5) in (1) yields

$$r_n(t) = \sum_{m=0}^{M-1} \sigma_p f_m(t) \exp\left\{ j\frac{\omega_c}{c}(x_{tm} + x_{rn})\sin\theta_p \right\},$$

$$n = 0, 1, \ldots, N-1. \tag{6}$$

From the argument of the exponential in (6), it can be seen that the MIMO radar appears to have phase centers located at the virtual locations $x_{tm} + x_{rn}$. Thus, the equivalent virtual array or coarray is defined as the set [24, 25]

$$C_S = \{\mathbf{z} : \mathbf{z} = \mathbf{x}_t + \mathbf{x}_r, \mathbf{x}_t \in S_T, \mathbf{x}_r \in S_R\} \tag{7}$$

where S_T and S_R are the sets of physical transmit and receive element phase centers, respectively. The maximum number of virtual elements that the coarray can have is MN, which can be achieved by proper placement of the transmit and receive antennas such that every pair of transmit and receive elements contributes to the formation of only one coarray element. For example, an N-element uniform linear receive array with spacing d and an M-element uniform linear transmit array with interelement spacing $Nd/2$ result in an MN-element uniform linear MIMO virtual array with an interelement spacing of d [24]. For such a MIMO radar system, the virtual array or coarray length is M times that of the corresponding SIMO radar system. This increased virtual array size results in improved cross-range resolution, thereby permitting better target localization.

We now examine how the concept of the virtual array or coarray extends to the case when wideband signals are used in a MIMO radar. Let $s_m(t)\exp\{j\omega_c t\}$ be the wideband signal emitted by the mth transmit element. Then, the baseband signal received at the nth receive element is of the form

$$z_n(t) = \sum_{m=0}^{M-1} \sigma_p s_m\left(t + \frac{(x_{tm} + x_{rn})\sin\theta_p}{c}\right)$$

$$\cdot \exp\left\{ j\frac{\omega_c}{c}(x_{tm} + x_{rn})\sin\theta_p \right\}. \tag{8}$$

Consider the Fourier transform $S_m(\omega)$ of the wideband signal $s_m(t)$, given by

$$s_m(t) = \frac{1}{2\pi} \int_{-\infty}^{\infty} S_m(\omega)\exp\{j\omega t\}d\omega. \tag{9}$$

Using the time-shift property of the Fourier transform, we obtain

$$s_m\left(t + \frac{(x_{tm} + x_{rn})\sin\theta_p}{c}\right)$$

$$= \frac{1}{2\pi} \int_{-\infty}^{\infty} S_m(\omega)\exp\left\{ j\omega \frac{(x_{tm} + x_{rn})\sin\theta_p}{c} \right\}\exp\{j\omega t\}d\omega. \tag{10}$$

Therefore, the frequency-domain representation of the underlying problem is obtained by using (8) and (10) as

$$z_n(t) = \sum_{m=0}^{M-1} \frac{\sigma_p}{2\pi} \int_{-\infty}^{\infty} S_m(\omega)$$
$$\cdot \exp\left\{ j\frac{(\omega + \omega_c)}{c}(x_{tm} + x_{rn})\sin\theta_p \right\} \exp\{j\omega t\}d\omega. \tag{11}$$

Considering the corresponding expression in (6) for narrowband operation and replacing the narrowband signal $f_m(t)$ by its Fourier transform $F_m(\omega)$, we obtain

$$r_n(t) = \sum_{m=0}^{M-1} \frac{\sigma_p}{2\pi} \int_{-\infty}^{\infty} F_m(\omega)$$
$$\cdot \exp\left\{ j\frac{\omega_c}{c}(x_{tm} + x_{rn})\sin\theta_p \right\} \exp\{j\omega t\}d\omega. \tag{12}$$

Comparing (11) and (12), we find that the expression in (11) for the wideband case is structurally the same as that for the narrowband case. However, the delay $(x_{tm} + x_{rn})\sin\theta_p/c$ now appears as a frequency-dependent phase delay. Considering the argument of the exponential in (11) and noting that, more precisely, the MIMO virtual array elements are located at $(x_{tm} + x_{rn})/\bar{\lambda}$, where $\bar{\lambda}$ is the wavelength corresponding to $\omega + \omega_c$, an explicit definition of the virtual array or coarray is required, which would dilate it by the factor $1/\bar{\lambda}$. That is, if C_S is the virtual array or coarray corresponding to a MIMO radar, then the dilated virtual array, denoted by $\bar{\lambda} \cdot C_S$ is given by [27]

$$\bar{\lambda} \cdot C_S = \left\{ \frac{\mathbf{z}}{\bar{\lambda}} : \mathbf{z} \in C_S \right\}. \tag{13}$$

For every constituent frequency of the signal bandwidth, we will have a corresponding dilated virtual array or coarray. Thus, for wideband operation, the MIMO virtual array is the union of all the dilated virtual arrays or coarrays corresponding to the various frequencies comprising the signal bandwidth.

Another important aspect of MIMO radar is the choice of signaling technique. In general, the waveforms emitted simultaneously from each transmit antenna can be orthogonal to facilitate separate processing of the measurements from each transmit and receive antenna pair. An alternate simpler approach for obtaining orthogonality is to use time multiplexing. This approach requires sequential emission of each transmitter, which demands more acquisition time compared with the simultaneous transmitter operation and thus can suffer from loss of coherence of the target response. On the other hand, sequential operation achieves perfect orthogonality, and unlike real-world orthogonal waveforms, does not suffer from degrading effects of nonvanishing cross correlations [23, 24]. Time multiplexing of the transmitters is a viable option for coherent MIMO operation in through-the-wall radar sensing applications due to the following two main reasons: 1) ground-based urban imaging radar systems are typically vehicle portable, which restricts the available real estate for deploying multiple antennas on the same platform; this, combined with the important constraint of low cost, results in deployment of far more receivers than wideband transmitters; and 2) indoor targets of interest, such as humans, move at low velocities. As a result, loss of coherence may not be an issue. The sequential transmit operation is a salient feature of two known TWRI systems; one is built by the Army Research Lab [3, 15] and the other by the Defense Research and Development Canada [28].

For simultaneous transmission signaling scheme, besides orthogonality, waveforms are required to have good autocorrelation and cross-correlation properties. There are many recent works in the literature that present design of orthogonal waveforms with good cross-transmitter and range estimation characteristics [29–32]. Any such set of orthogonal waveforms can be employed in through-the-wall and urban radar sensing applications. In Section IV, we evaluate the performance of one set of simultaneous orthogonal waveforms for use in the particular MIMO radar system employed for real data collection and compare it to that of the sequential signaling scheme.

III. CHANGE DETECTION

We first develop the signal model for wideband MIMO operation with M transmitters and N receivers under coherent integration. Let $s_m(t)$ be the wideband signal used by the mth transmitter for interrogating the scene. For notational simplicity, the carrier term is not separately considered and each wideband signal is assumed to have a bandwidth B Hz centered at ω_c. The signal duration T_s is assumed to be less than the pulse repetition interval T_s. Assuming coherent integration of K pulses, the coherent integration interval becomes KT_r. For the case of a single-point target of reflectivity σ_p, located at $\mathbf{x}_p = (x_p, y_p)$, the kth pulse emitted by the mth transmitter is received at the nth receiver in the form

$$z_{mn}(t,k) = \sigma_p s_m(t - kT_r - \tau_{p,mn}) \tag{14}$$

where $\tau_{p,mn}$ is the propagation delay for the signal to travel between the mth transmitter, the target at $\mathbf{x}_p$, and the nth receiver. It is assumed that we deal with targets of constant radar cross section over the range of the used frequencies and target aspect angles. For through-the-wall propagation, $\tau_{p,mn}$ will comprise the components corresponding to traveling distances before, through, and after the wall [33]. The output of the nth receiver, due to simultaneous transmission

from all M transmit elements, is given by

$$z_n(t,k) = \sum_{m=0}^{M-1} z_{mn}(t,k) = \sum_{m=0}^{M-1} \sigma_p s_m(t - kT_r - \tau_{p,mn}).$$

(15)

The received signal is passed through a bank of filters with impulse responses $h_m(t)$, $m = 0, 1, \ldots, M-1$, matched to the transmit waveforms. As the set of transmit waveforms is orthogonal, i.e., $\int_0^{T_r} s_m(t) s_l^*$ $\cdot (t + \tau) dt = 0$ for any τ, where $m \neq l$, $m, l = 0, 1, \ldots, M-1$, the output of the filter matched to the mth transmit waveform can be expressed as

$$z_{mn}^{MF}(t,k) = z_n(t,k) * h_m(t)$$

$$= z_{mn}(t,k) * h_m(t) = \int_0^{T_r} h_m(u) z_{mn}(t - u, k) du$$

(16)

where $h_m(t) = s_m^*(-t)$. With K pulses coherently integrated, we obtain

$$z_{mn}^{CI}(t) = \sum_{k=0}^{K-1} z_{mn}^{MF}(t,k).$$

(17)

To generate an image of the scene being interrogated, the MN outputs corresponding to the operation of M transmitters and N receivers are processed as follows. The region of interest is divided into a finite number of pixels in x and y, where x and y represent the cross-range and downrange, respectively. The composite signal corresponding to the pixel, located at $\mathbf{x}_q = (x_q, y_q)$, is obtained by summing time delayed versions of the MN outputs of the M matched filters applied to each of the N receivers

$$z_q(t) = \sum_{m=0}^{M-1} \sum_{n=0}^{N-1} z_{mn}^{CI}(t + \tau_{q,mn})$$

(18)

where $\tau_{q,mn}$ is the focusing delay applied to the output of the mth matched filter at the nth receiver. Additional weighting can be applied during the summation operations of (18) to control the sidelobe level of the transmit-receive array pattern of the MIMO system. Substituting from (16) and (17) in (18) yields

$$z_q(t) = \sum_{m=0}^{M-1} \sum_{n=0}^{N-1} \sum_{k=0}^{K-1} \int_0^{T_r} h_m(u) z_{mn}(t + \tau_{q,mn} - u, k) du.$$

(19)

The complex amplitude image value $I(\mathbf{x}_q)$ for the pixel at $\mathbf{x}_q$ is obtained by sampling the signal $z_q(t)$ at time $t = 0$. That is,

$$I(\mathbf{x}_q) = z_q(t)|_{t=0}.$$

(20)

The process described by (18)–(20) is repeated for all pixels in the image to generate the composite image of the scene. The general case of multiple targets can be obtained by superposition of target reflections [33, 34].

For the case of time multiplexing of the M transmitters, a single wideband transmit waveform $s(t)$ is employed. In this case, the nth received signal with the mth transmitter active can be expressed as

$$z_{mn}(t,k) = \sigma_p s(t - mKT_r - kT_r - \tau_{p,mn})$$

(21)

where the factor mKT_r indicates the additional time required for data collection when the mth transmitter becomes active in a sequential order. It is assumed that the transmitters transmit their pulses in contiguous time intervals, each of length KT_r. The nth received signal is passed through a matched filter with impulse response $h(t) = s^*(-t)$ and coherently integrated. That is,

$$z_{mn}^{CI}(t) = \sum_{k=0}^{K-1} z_{mn}^{MF}(t,k)$$

(22)

$$z_{mn}^{MF}(t,k) = z_{mn}(t,k) * h(t) = \int_0^{T_r} h(u) z_{mn}(t - u, k) du.$$

In this case, the composite signal $z_q(t)$ and the complex amplitude image value $I(\mathbf{x}_q)$ for the pixel at $\mathbf{x}_q$ are given by (19) and (20), respectively, with $h_m(t)$ replaced by $h(t)$ and $z_{mn}(t,k)$, given by (21). Thus, the same radar imaging capability in terms of cross-range resolution is achieved as that for simultaneous transmissions, while the data collection time is increased by a factor of M.

In its simplest form, the MTI processing is achieved by using the radar images corresponding to two data frames, which may be consecutive or separated by one or more data frames. For simultaneous transmissions, a data frame length T_f is equal to the coherent integration interval, i.e., $T_f = KT_r$, whereas in case of time multiplexing, a data frame length is equal to M coherent integration intervals, i.e., $T_f = MKT_r$. Let $\{I^{(t)}(\mathbf{x}_q)\}_{q=0}^{Q-1}$ and $\{I^{(t+LT_f)}(\mathbf{x}_q)\}_{q=0}^{Q-1}$ be the radar images corresponding to the data collected over the two frames, where Q is the number of pixels in each image and L denotes the number of frames between the two acquisitions. It is noted that $L = 1$ represents the case in which the two acquisitions are performed over consecutive frames. The timing interval for each data frame is assumed to be a fraction of a second so that the moving target appears stationary during data collection. Coherence is required only over each individual frame and not necessarily across the two frames.

CD can be performed in two ways [15–19]. In the first approach, complex amplitude image values corresponding to the two data frames are subtracted on a pixel-by-pixel basis. The second approach involves subtraction of image pixel intensity values corresponding to different data frames, followed by a zero threshold operation to suppress the reference
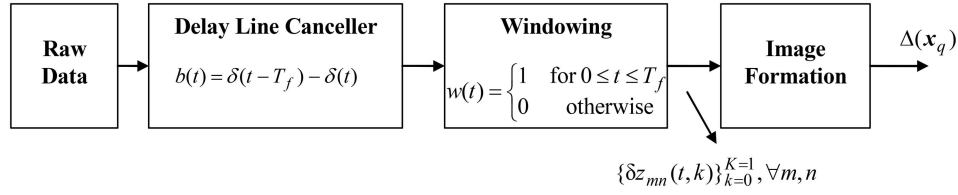
Fig. 2.   Block diagram of data domain CD approach (prebeamforming CD), equivalent to complex amplitude image subtraction.
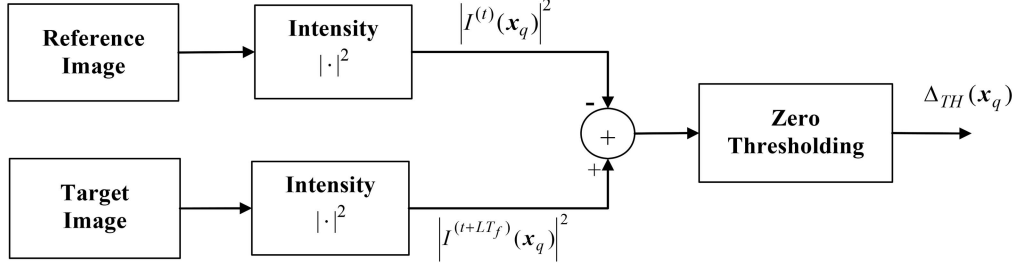

Fig. 3.   Block diagram of intensity image CD approach (postbeamforming CD).

image. For the first approach, the motion detection image can be expressed as follows:

$$\Delta(\mathbf{x}_q) = I^{(t+LT_f)}(\mathbf{x}_q) - I^{(t)}(\mathbf{x}_q), \qquad q = 0, 1, \ldots, Q-1. \tag{23}$$

Substituting from (19) and (20), we can rewrite (23) for the case of simultaneous transmission of orthogonal waveforms, as

$$\Delta(\mathbf{x}_q) = \sum_{m=0}^{M-1} \sum_{n=0}^{N-1} \sum_{k=0}^{K-1} \int_0^{T_r} h_m(u) \delta z_{mn}(t + \tau_{q,mn} - u, k) du \Bigg|_{t=0} \tag{24}$$

where

$$\delta z_{mn}(t, k) = z_{mn}(t - LKT_r, k) - z_{mn}(t, k)$$
$$= z_{mn}(t, k) * [\delta(t - LKT_r - kT_r) - \delta(t - kT_r)] \tag{25}$$

and $z_{mn}(t, k)$ is defined in (14). The corresponding equations for time multiplexing of M transmitters are

$$\Delta(\mathbf{x}_q) = \sum_{m=0}^{M-1} \sum_{n=0}^{N-1} \sum_{k=0}^{K-1} \int_0^{T_r} h(u) \delta z_{mn}(t + \tau_{q,mn} - u, k) du \Bigg|_{t=0} \tag{26}$$

with

$$\delta z_{mn}(t, k) = z_{mn}(t - LMKT_r, k) - z_{mn}(t, k)$$
$$= z_{mn}(t, k) * [\delta(t - LMKT_r - kT_r) - \delta(t - kT_r)] \tag{27}$$

and $z_{mn}(t, k)$ given by (21). From (24)–(27), we observe that for both signaling schemes, the subtraction of complex amplitude image values for each pixel amounts to subtraction of the received data corresponding to the two frames for each range bin, followed by image formation. Equations (25) and (27) provide the equivalent DLC representation for CD

directly in the data domain, i.e., prebeamforming CD. A block diagram of the data domain CD algorithm implementation is provided in Fig. 2. Note that the windowing operation in the figure ensures application of the algorithm over data frames of length T_f.

The block diagram of Fig. 2 is a two-frame DLC, reminiscent of the commonly used two-pulse DLC for clutter filter in range-Doppler radars [11]. More frames can be used in CD leading to multiple frames DLC, which is similar to three-pulse or higher-pulse DLC. However, unlike range-Doppler radar systems, in which higher-order clutter filters provide flexibility in trading off clutter suppression with Doppler frequency magnitude, there are no clear advantages of using multiple frames in CD for the underlying problem. Hunt [19] suggested averaging multiple frames, only to emphasize the stationary targets.

The second CD approach involving intensity images is depicted in Fig. 3. In this case, the intensity images corresponding to the two data frames are first computed. Then, a difference image is generated by a pixel-by-pixel subtraction of the intensity images as

$$\Delta(\mathbf{x}_q) = |I^{(t+LT_f)}(\mathbf{x}_q)|^2 - |I^{(t)}(\mathbf{x}_q)|^2, \qquad q = 0, 1, \ldots, Q-1. \tag{28}$$

The final motion detection image is obtained by a zero threshold operation

$$\Delta_{TH}(\mathbf{x}_q) = \begin{cases} \Delta(\mathbf{x}_q), & \text{if } \Delta(\mathbf{x}_q) \geq 0 \\ 0 & \text{otherwise} \end{cases}. \tag{29}$$

This threshold results in the target appearing in the final motion detection image only at the position it was occupying during acquisition of the second (test) data frame, because the target image at position corresponding to the first (reference) data frame appears as a negative value after intensity subtraction and is thus removed. Unlike the complex amplitude
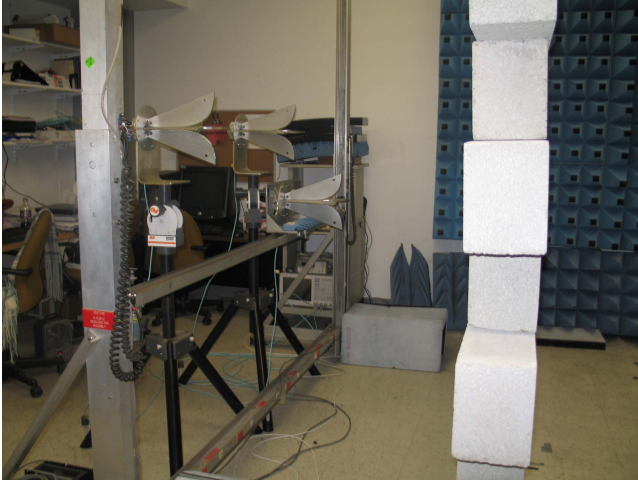
Fig. 4. MIMO system used for data collection.

Fig. 5. (a) Dilated coarray at 2 GHz. (b) Wideband coarray.

image subtraction, there is no equivalent data domain representation for the intensity image subtraction or postbeamforming CD approach due to the nonlinearity of the modulus function in (28). However, the DLC framework can still be applied. The image intensity at each pixel can be viewed as a nonlinear function of the data in the respective frame, and the subtraction, implied by the DLC, is performed between two corresponding pixels separated by one or multiple frames.

The aforementioned CD schemes, though presented for motion detection, can also be applied for detection of stationary targets in the presence of clutter and noise [16]. If a target-free background image of the scene being interrogated is available (feasible when the radar system is being used for long-term surveillance), it can be subtracted (complex amplitude or intensity pixel subtraction) from an image of the same scene acquired at a later time that may contain a target of interest, thus rendering background subtraction as a special case of CD.

IV. EXPERIMENTAL RESULTS

A wideband MIMO through-the-wall radar system was set up in the Radar Imaging Lab at Villanova University. A stepped-frequency CW signal, consisting of 101 frequency steps of size 10 MHz, covering the 1.5-2.5 GHz band was chosen for imaging. The bandwidth of 1 GHz provides a range resolution of 15 cm, and the 10-MHz frequency step allows 15-m unambiguous range, which is roughly three times the length of the room being imaged. An Agilent network analyzer, model ENA 5071B, was used for signal synthesis and data collection. A horn antenna, model ETS-Lindgren 3164-04, with an operational bandwidth from 0.7 to 6 GHz, was mounted on a field probe scanner to synthesize an 11-element uniform receive line array with an interelement spacing of 7.5 cm. The interelement spacing on receive was selected as $\lambda_c/2$, where λ_c is
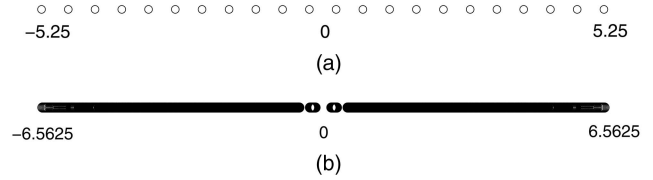
the wavelength corresponding to the 2-GHz center frequency. Two horn antennas (model ETS-Lindgren 3164-04), mounted on tripods and placed slightly above and on either side of the receive array, were used as transmitters, as shown in Fig. 4. The first transmitter was placed 3.75 cm to the right of the rightmost receiver, while the second transmitter was positioned at 3.75 cm to the left of the leftmost receiver. A 10×8-ft wall segment was constructed using 0.14-m-thick solid concrete blocks with a dielectric constant of 7.66. The receive array was at a standoff distance of 1.05 m from the wall, whereas the transmitters were positioned 1.33 m in downrange from the wall.

The employed transmit and receive array apertures achieve a 22-element uniform linear virtual array or coarray at 2 GHz of length $10.5\lambda_c$. That is, the phase center of the jth coarray element is given by

$$\mathbf{z}_j = -5.25\lambda_c + j\frac{\lambda_c}{2} = (-5.25 + j0.5)\lambda_c, \qquad j = 0, 1, \ldots, 21. \tag{30}$$

Equivalently, after normalization by λ_c, the dilated virtual array extent at 2 GHz is 10.5, as shown in Fig. 5(a). As discussed earlier, because the coarray locations are scaled by 1/wavelength corresponding to the various radar frequencies, operating at multiple frequencies adds additional points at specific locations in the coarray. Thus, for wideband stepped-frequency radar system, the virtual array or coarray is the union of the dilated coarrays corresponding to all 101 frequencies constituting the 1-GHz bandwidth. Expressing the equispaced 101 frequencies covering the 1-GHz signal bandwidth as

$$f_i = \left(1 + i\frac{0.01}{2}\right)f_c, \quad i = -50, -49, \ldots, 50, \qquad f_c = 2 \text{ GHz} \tag{31}$$

the corresponding wideband virtual array C_{WB} is given by

$$
\begin{aligned}
C_{WB} &= \bigcup_{i=-50}^{50} \lambda_i \cdot C_S = \bigcup_{i=-50}^{50} \bigcup_{j=0}^{21} \frac{\mathbf{z}_j}{\lambda_i} \\
&= \bigcup_{i=-50}^{50} \bigcup_{j=0}^{21} \frac{\mathbf{z}_j(1 + i0.005)}{\lambda_c}
\end{aligned}
\tag{32}
$$

with $\mathbf{z}_j$ defined in (30). From (32), we observe that operation at frequencies lower than the center frequency, corresponding to negative values of
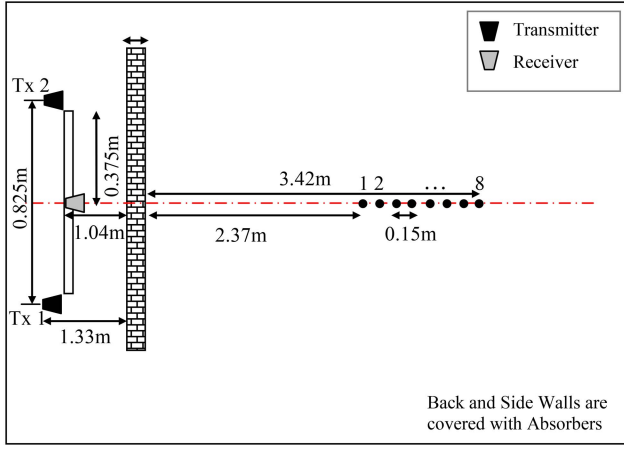
Fig. 6.   Layout of scene and target trajectory.

(a)

(b)

Fig. 7.   Beamformed images using MIMO radar for target at position (a) 3 and (b) 4 (consecutive range cells).

the index i, contracts the coarray in (30), while higher operational frequencies expand the coarray. Figure 5(b) shows the wideband virtual array, which is a linear array of extent 13.125.

Under SIMO operation using a single transmitter and all 11 receivers, the length of the virtual array or coarray at 2 GHz is equal to that of the receive array, and the corresponding wideband SIMO virtual linear array has an extent equal to 52.38% of the length of the wideband MIMO virtual array. In other words, the MIMO operation will certainly result in a better cross-range resolution compared with the SIMO case and, as such, is expected to provide improved localization of the targets.

To illustrate the performance of CD under complex and intensity image DLCs and with and without the MIMO processing, we consider two different moving target experiments. In the first experiment, a human walks away from the front wall in an empty room, following a straight-line path. Because simultaneous data cannot be collected at all receive locations due to the synthetic nature of the receive aperture, eight different target positions were considered, separated by 15 cm, along the trajectory, as illustrated in Fig. 6. Data was collected for all eight positions, with the target stationary at each position, using the MIMO system with time multiplexing of the transmitters.

We first consider the case in which the person moves from position 3 to position 4. That is, the two acquisitions are performed over consecutive frames. Figures 7(a) and (b) show the beamformed images with the MIMO radar using the data corresponding to positions 3 and 4, respectively. In these figures and all subsequent figures in this section, we plot the image intensity with the maximum intensity value in each image normalized to 0 dB. Both images show strong reflections from the front wall, rendering target returns hard to detect in either image. Figure 8(a) shows the result of CD wherein the complex radar image of Fig. 7(a) is subtracted from the complex image of Fig. 7(b). We observe that all stationary background,
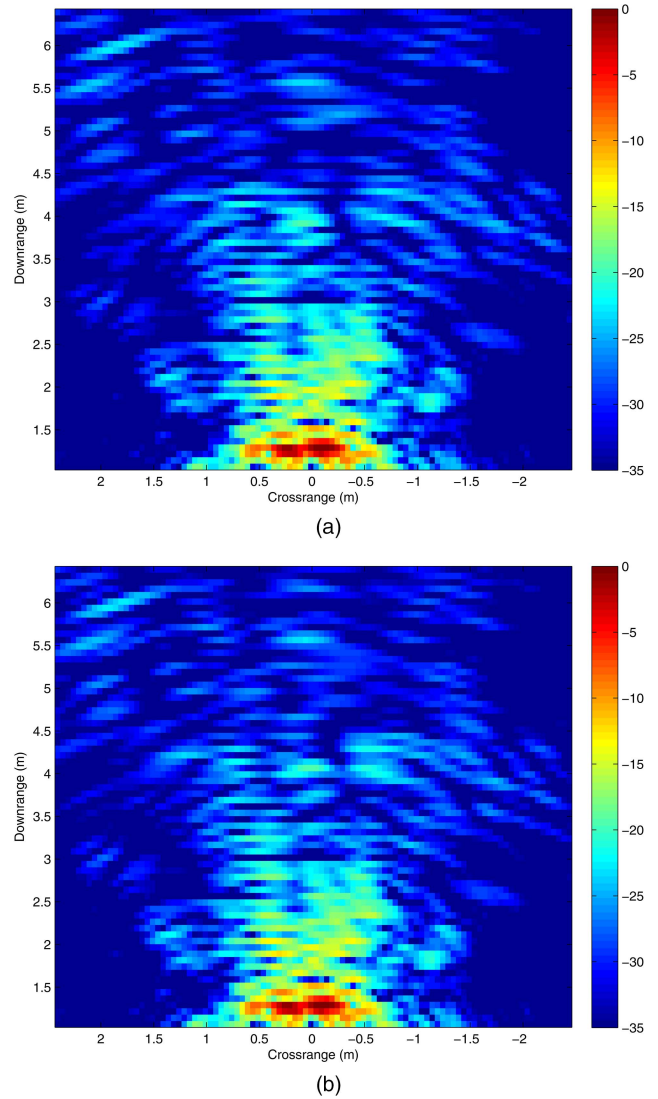
including the front wall, has been eliminated from the image, and the target undergoing motion has been detected. Because the target appears in two consecutive range cells, no clear target displacement is observed, and the target image appears blurred. For comparison, the CD image resulting from the SIMO operation (transmitter 1 only) is provided in Fig. 8(b). Again, the target is clearly detected and appears blurred. However, as expected, the SIMO operation results in an inferior cross-range resolution compared with the MIMO case. Prior to normalization, the maximum pixel intensity of the MIMO CD image in Fig. 8(a) was about 5.68 dB higher than that of the SIMO image in Fig. 8(b). The corresponding CD results under intensity image DLC for both MIMO and SIMO operations are presented in Fig. 9. We observe that, for both SIMO and MIMO radar operations, the intensity image DLC removes most of the imaged target in the case of consecutive range
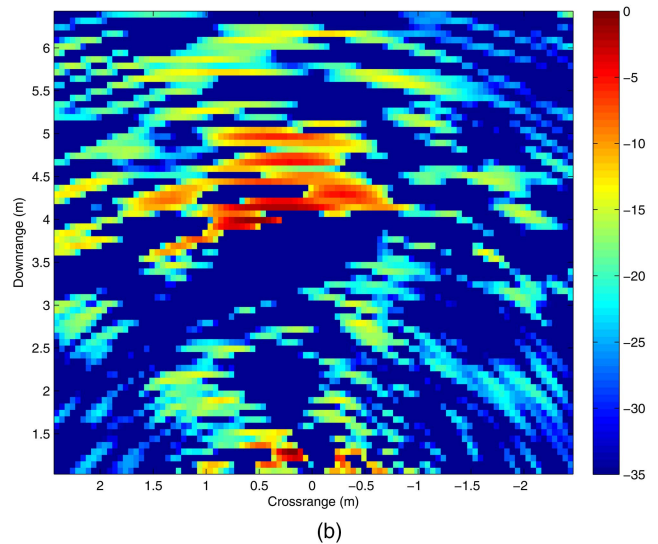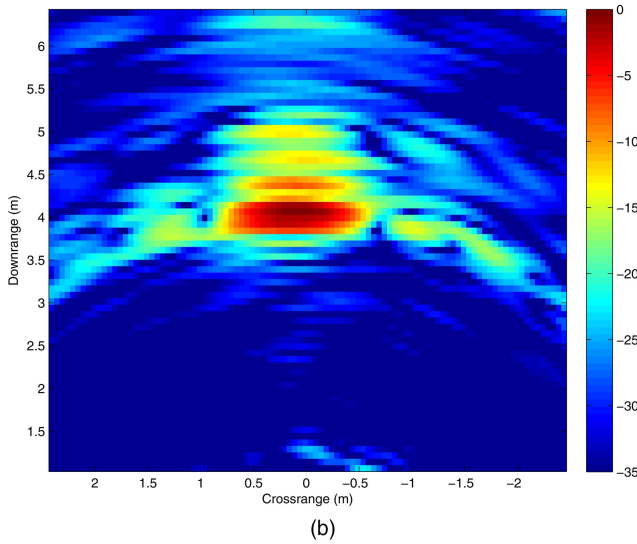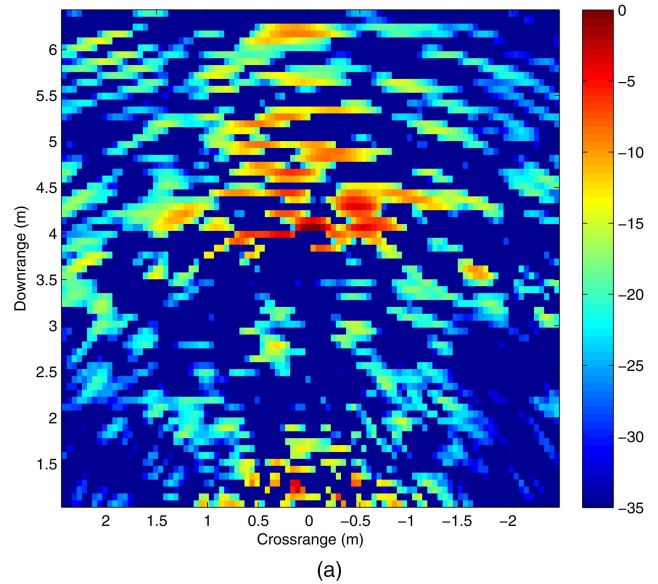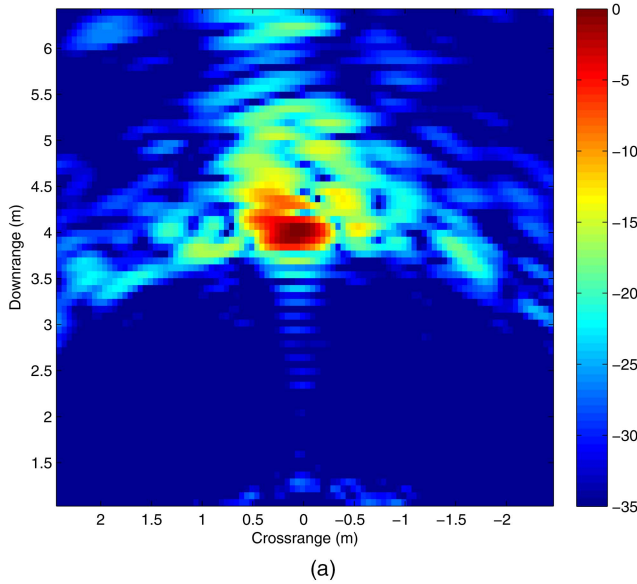
Fig. 8. Images after CD under complex image DLC of human walking from position 3 to position 4 using (a) MIMO radar and (b) SIMO radar.

Fig. 9. Images after CD under intensity image DLC of human walking from position 3 to position 4 using (a) MIMO radar and (b) SIMO radar.

cell acquisitions. Moreover, due to the nonlinearity of the modulus function, the stationary background in the image is, in general, different for each data acquisition, thereby causing the background to be only partially cancelled out under intensity image DLC [19]. As a result, stronger artifacts than those of the complex image DLC can be clearly observed. The ability to detect the target in the change detected image is, therefore, reduced under intensity image DLC as compared with complex image DLC.

Next, we investigate the performance of the various schemes for both MIMO and SIMO operations under large target displacement between consecutive acquisitions. Consider the case in which the person moves from position 1 to position 4. Figure 10 shows the beamformed image with the MIMO radar using the data corresponding to position

1, while the image corresponding to position 4 is shown in Fig. 7(b). Again, the target returns are hard to detect. Figure 11(a) shows the result of CD wherein the complex radar image of Fig. 10 is subtracted from the complex image of Fig. 7(b). Because the target undergoes large range migration, the moving target presents itself as two targets in the image. For comparison, the CD image resulting from the SIMO operation (transmitter 1 only) is provided in Fig. 11(b). Similar results are obtained, though with an inferior cross-range resolution compared with the MIMO case. The CD results under intensity image DLC for the large target displacement case under both MIMO and SIMO operations are presented in Fig. 12. We observe that for both SIMO and MIMO radar operations, the intensity image DLC retains the target at position 4 and removes the target at position 1.
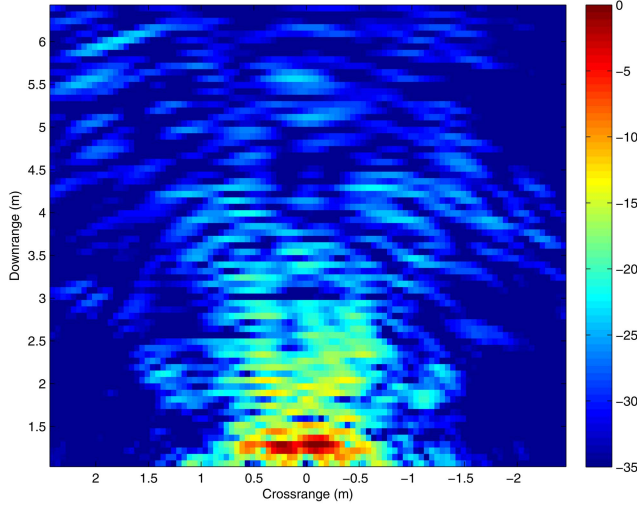
Fig. 10. Beamformed image using MIMO radar for target at position 1.
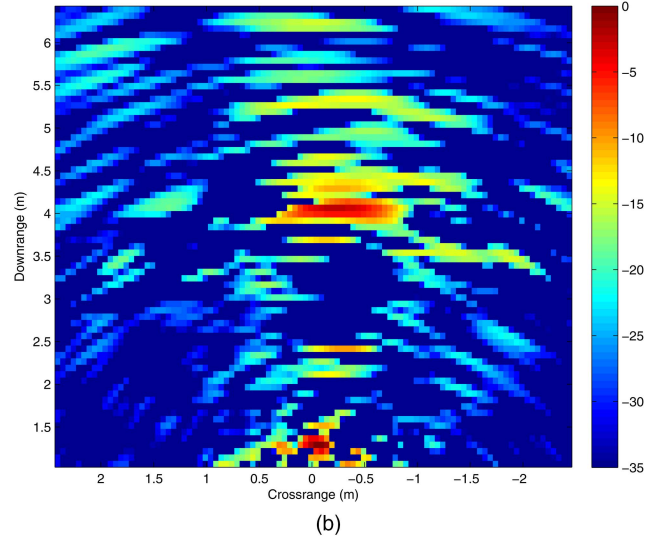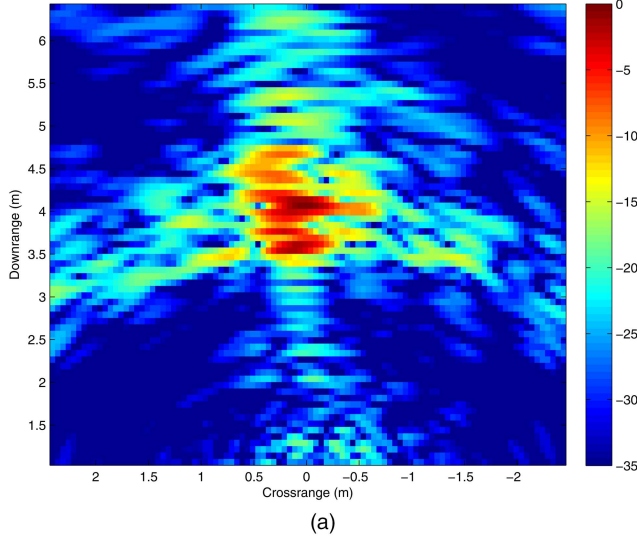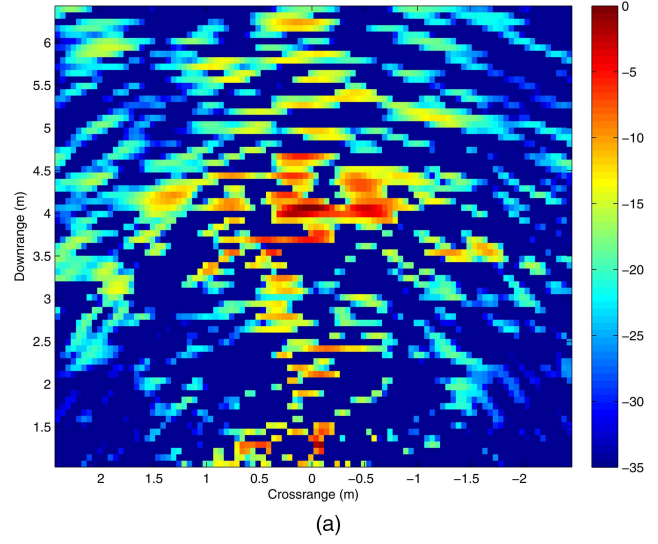

(a)

(a)

(b)

Fig. 12. Images after CD under intensity image DLC of human walking from position 1 to position 4 using (a) MIMO radar and (b) SIMO radar.
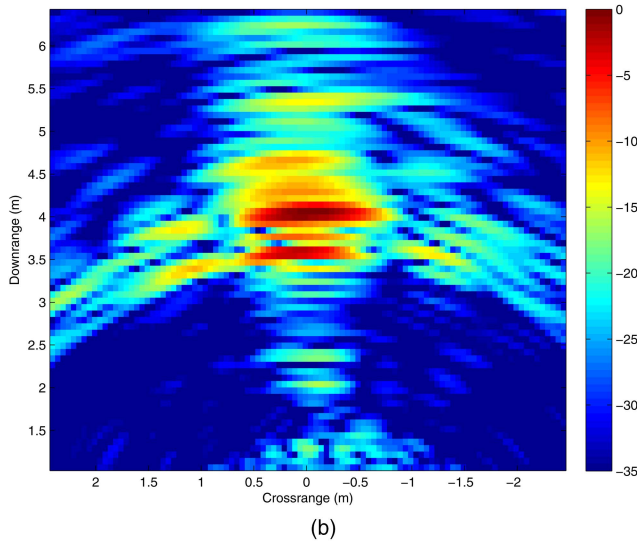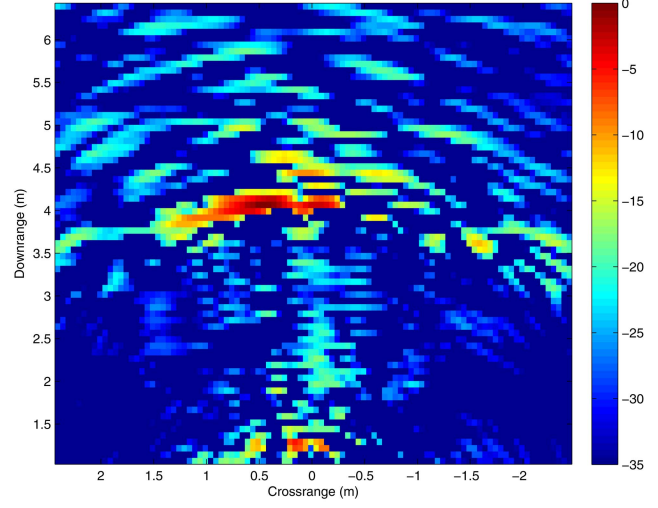

(b)

Fig. 11. Images after CD under complex image DLC of human walking from position 1 to position 4 using (a) MIMO radar and (b) SIMO radar.

However, similar to the small target displacement case, the artifacts resulting from the background not being totally canceled out render target detection difficult.

For further elaborations on the difference in performance of the proposed CD schemes, we consider two humans walking side by side away from the front wall in an empty room. The scene layout and the trajectory of the targets in the second experiment is the same as that for the first experiment (see Fig. 6). Data were collected for all eight positions of the targets with both targets stationary at each position. Figures 13(a) and (b) show the result of complex image based CD using the MIMO and SIMO (transmitter 1 only) radar, respectively, wherein the radar image corresponding to the targets at position 4 is subtracted from the image corresponding to position 3. We observe from Fig. 13(a) that both targets undergoing motion have been detected. As for the single target case, each target appears in
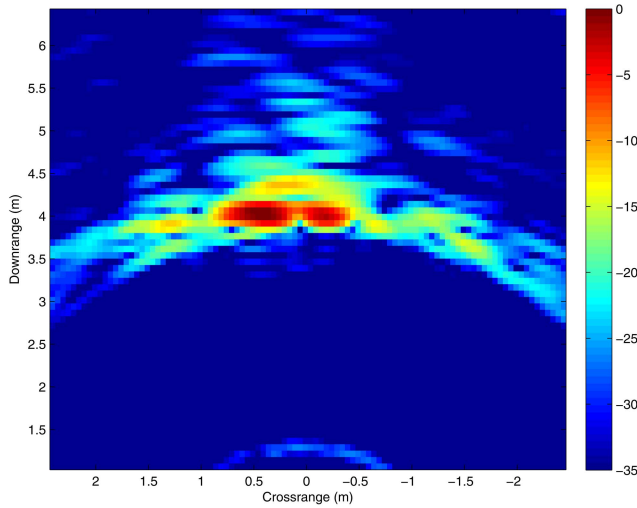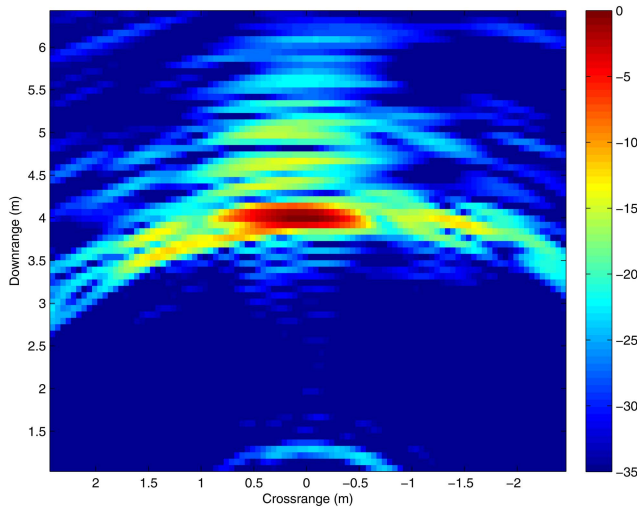
Fig. 13. Images after CD under complex image DLC of humans walking side by side from position 3 to position 4 using (a) MIMO radar and (b) SIMO radar.

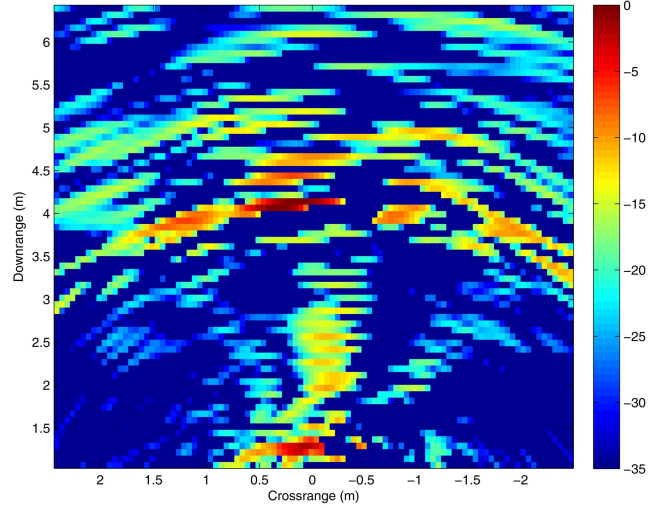Fig. 14. Images after CD under intensity image DLC of humans walking side by side from position 3 to position 4 using (a) MIMO radar and (b) SIMO radar.

consecutive range cells and appears blurred in the CD image. On the other hand, as seen in Fig. 13(b), the SIMO operation has not been able to resolve the two targets because of its inferior cross-range resolution compared with the MIMO case. The corresponding CD results under intensity image DLC for both MIMO and SIMO operations are presented in Fig. 14. Similar to what was observed in the single target case, the intensity image DLC removes most of the imaged targets for SIMO and MIMO radar operations, and the images have a high degree of artifacts compared with their complex image DLC counterparts.

For the case when the persons move from position 3 to position 7, i.e., large displacement, the complex image DLC results and the intensity image DLC results under both MIMO and SIMO (transmitter 1 only) radar operations are provided in Figs. 15 and 16, respectively. From Fig. 15(a), we observe that each moving target presents itself as two targets

in the MIMO image. On the other hand, the SIMO radar is unable to resolve the humans walking side by side, and only a single imaged target appears at both positions 3 and 7, as depicted in Fig. 15(b). For the intensity image DLC results in Fig. 16, only the imaged targets at position 7 are retained, albeit with the strong artifacts compared with the corresponding complex image DLC.

To compare the performance of the sequential transmission signaling scheme with simultaneous transmission signaling scheme, the data sets corresponding to positions 3 and 7 for the two target experiment were preprocessed in order to emulate simultaneous operation of the transmitters using up and down chirp waveforms. The preprocessing at each receiver involved 1) synthesizing the effect of transmitting up and down chirps by applying appropriate spectral weightings to the received stepped-frequency CW signals corresponding to
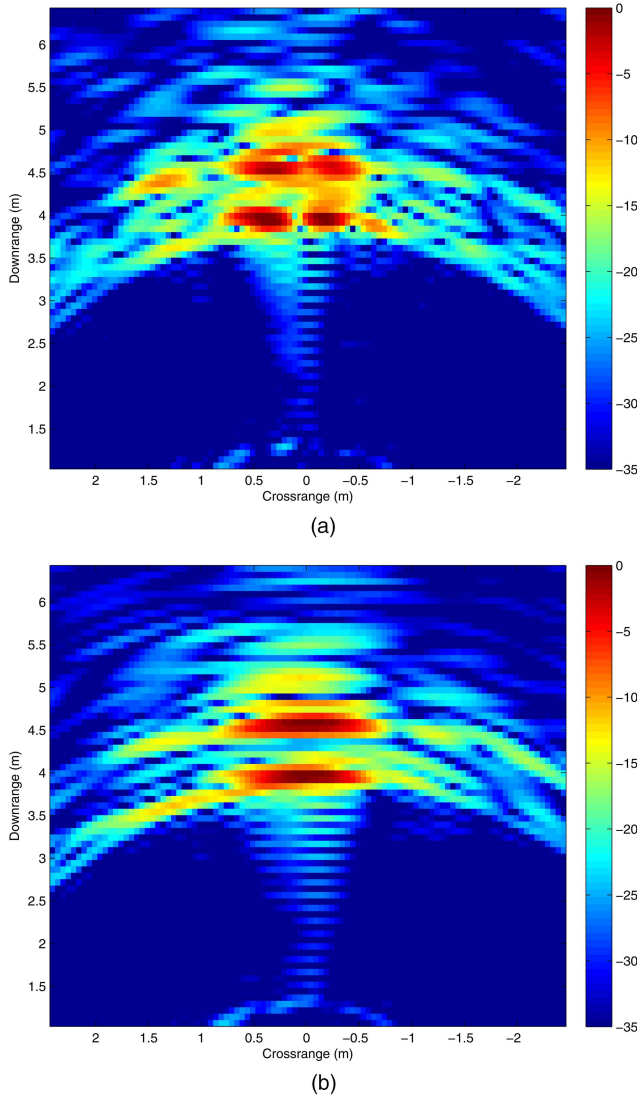
Fig. 15. Images after CD under complex image DLC of humans walking side by side from position 3 to position 7 using (a) MIMO radar and (b) SIMO radar.

Fig. 16. Images after CD under intensity image DLC of humans walking side by side from position 3 to position 7 using (a) MIMO radar and (b) SIMO radar.

the two transmitters, 2) adding up the weighted returns, and 3) passing the summed signal through a bank of filters matched to the up and down chirps. Figures 17(a) and (b) show the corresponding CD images for the complex image DLC and intensity image DLC techniques. Compared with the corresponding sequential transmission results of Figs. 15(a) and 16(a), the effects of nonvanishing cross-correlations are clearly visible in both images in Fig. 17. In fact, for the intensity image DLC, the artifacts due to incomplete background subtraction are much more pronounced due to nonvanishing cross-correlations and result in a highly cluttered image compared with the corresponding sequential transmission image of Fig. 16(a).

V. CONCLUSION

In this paper, MTI for detecting slow-moving personnel behind walls was achieved by a radar imaging system that allows MIMO configuration, which provides improved localization and cross-range resolution of the moving targets. We provided analytical formulation of MIMO-based CD and examined the system performance when clutter removal was performed pre- and postbeamforming. Lab experiments conducted in the Radar Imaging Facility at the Center for Advanced Communications, Villanova University, were used to validate the proposed approaches under both large and small target displacements over consecutive acquisitions. The results clearly showed the superior cross-range resolution of the MIMO radar compared with the SIMO radar for the considered cases. For large target displacements, the prebeamforming CD scheme showed two sets of imaged targets corresponding to the target positions at the two data acquisitions, whereas the postbeamforming CD, due to zero thresholding, retained only one set of imaged targets,
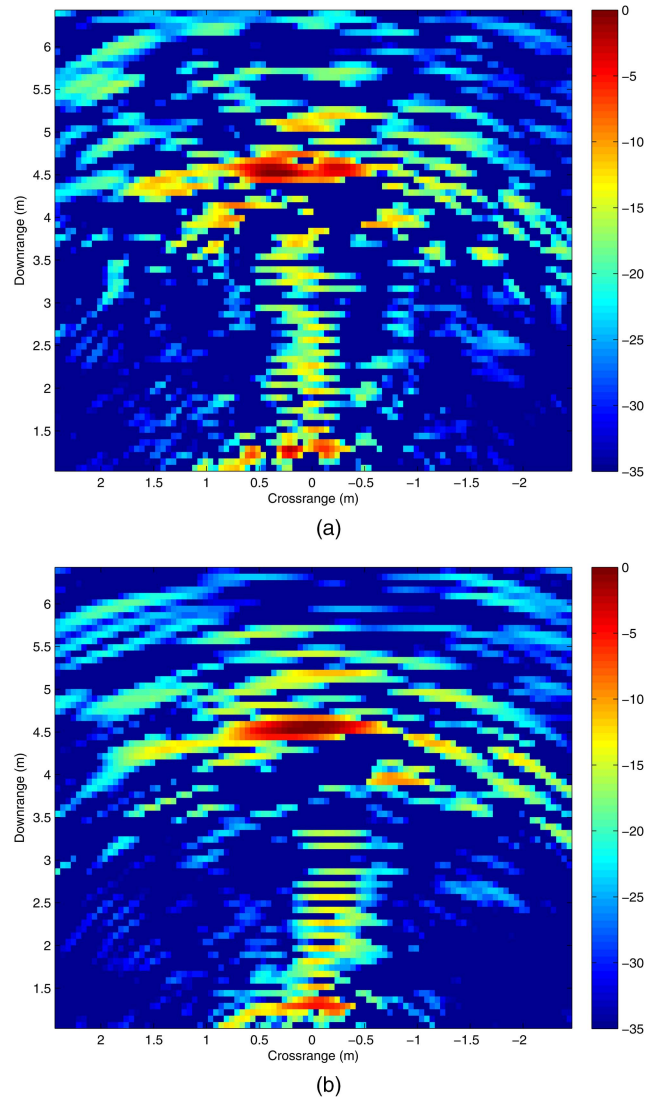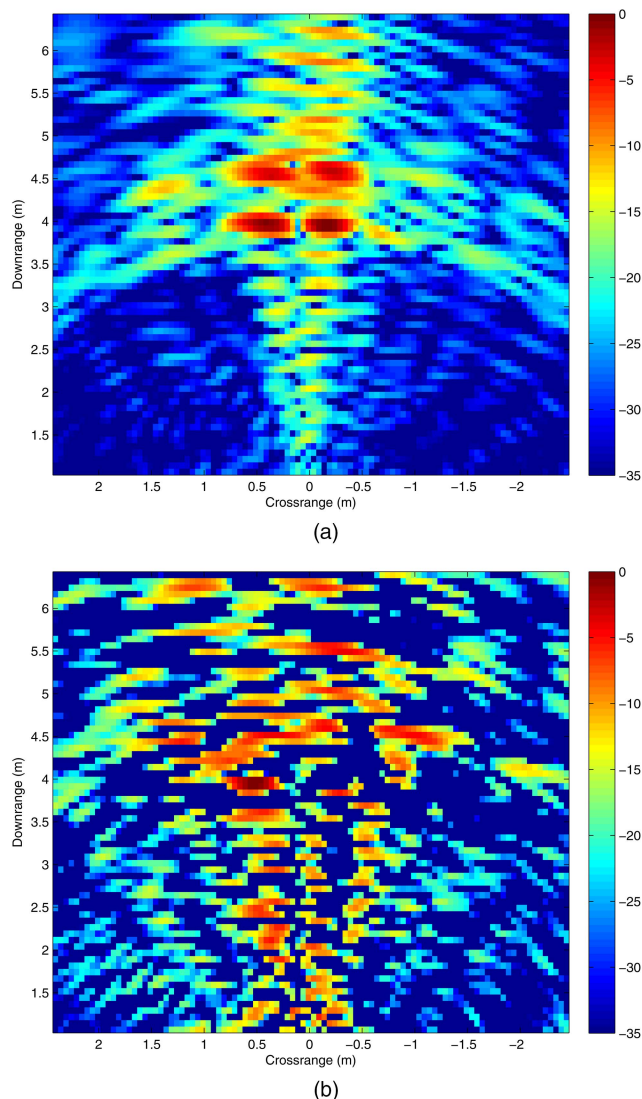
(a)

(b)

Fig. 17.   Images after CD of humans walking side by side from position 3 to position 7 using simultaneous transmissions with up and down chirps under (a) complex image DLC and (b) intensity image DLC.

though with significantly more artifacts. For small target displacements, the prebeamforming CD has better performance than the postbeamforming CD.

REFERENCES

[1]   Amin, M. G. (Ed.)
        Through-the-Wall Radar Imaging.
        Boca Raton, FL: CRC Press, 2010.
[2]   Amin, M. and Sarabandi, K. (Eds.)
        Special issue on remote sensing of building interior.
        IEEE Transactions on Geoscience and Remote Sensing, **47**, 5 (May 2009), 1270–1420.
[3]   Martone, A., Ranney, K., and Innocenti, R.
        Through-the-wall detection of slow-moving personnel.
        Proceedings of the SPIE—Radar Sensor Technology XIII, **7308** (Apr. 2009), pp. 73080Q1–73080Q12.

[4]   Ram, S. S. and Ling, H.
        Through-wall tracking of human movers using joint Doppler and array processing.
        IEEE Geoscience and Remote Sensing Letters, **5**, 3 (July 2008), 537–541.
[5]   Amin, M. (Ed.)
        Special issue on advances in indoor radar imaging.
        Journal of the Franklin Institute, **345**, 6 (Sept. 2008), 556–722.
[6]   Dogaru, T. and Le, C.
        Validation of Xpatch computer models for human body radar signature.
        U.S. ARL, Adelphi, MD, Tech. Rep. ARL-TR-4403, Mar. 2008.
[7]   Lai, C. P. and Narayanan, R. M.
        Through-wall imaging and characterization of human activity using ultrawideband (UWB) random noise radar.
        Proceedings of the SPIE—Sensors and C3I Technologies for Homeland Security and Homeland Defense, **5778** (May 2005), pp. 186–195.
[8]   Yoon, Y-S. and Amin, M. G.
        Spatial filtering for wall-clutter mitigation in through-the-wall radar imaging.
        IEEE Transactions on Geoscience and Remote Sensing, **47**, 9 (2009), 3192–3208.
[9]   Tivive, F., Amin, M., and Bouzerdoum, A.
        Wall clutter mitigation based on eigen-analysis in through-the-wall radar imaging.
        In *Proceedings of the 17th International Conference on Digital Signal Processing (DSP)*, Corfu, Greece, July 2011.
[10] Dehmollaian, M. and Sarabandi, K.
        Refocusing through building walls using synthetic aperture radar.
        IEEE Transactions on Geoscience and Remote Sensing, **46**, 6 (2008), 1589–1599.
[11] Skolnik, M.
        Introduction to Radar Systems (3rd ed.).
        New York: McGraw Hill, 2001.
[12] Ram, S. S., et al.
        Doppler-based detection and tracking of humans in indoor environments.
        Journal of the Franklin Institute, **345**, 6 (Sept. 2008), 679–699.
[13] Thayaparan, T., Stankovic, L., and Djurovic, I.
        Micro-Doppler human signature detection and its application to gait recognition and indoor imaging.
        Journal of the Franklin Institute, **345**, 6 (Sept. 2008), 700–722.
[14] Orovic, I., Stankovic, S., and Amin, M.
        A new approach for classification of human gait based on time-frequency feature representations.
        Signal Processing, **91**, 6 (June 2011), 1448–1456.
[15] Ranney, K., et al.
        Recent MTI experiments using ARL's synchronous impulse reconstruction (SIRE) radar.
        Proceedings of the SPIE—Radar Sensor Technology XII, **6947** (Apr. 2008), pp. 694708-1–694708-9.
[16] Moulton, J., et al.
        Target and change detection in synthetic aperture radar sensing of urban structures.
        In *Proceedings of the IEEE Radar Conference*, Rome, Italy, May 2008.
[17] Soldovieri, F., Solimene, R., and Pierri, R.
        A simple strategy to detect changes in through the wall imaging.
        Progress in Electromagnetics Research M, **7** (2009), 1–13.

[18]   Hunt, A. R.
         Use of a frequency-hopping radar for imaging and motion
         detection through walls.
         IEEE Transactions on Geoscience and Remote Sensing, **47**,
         5 (May 2009), 1402–1408.

[19]   Zhang, Y. D. and Hunt, A.
         Image and localization of behind-the-wall targets using
         collocated and distributed apertures.
         In *Through-the-Wall Radar Imaging*, Boca Raton, FL:
         CRC Press, 2010, ch. 4.

[20]   Maaref, N., et al.
         A study of UWB FM-CW radar for the detection of
         human beings in motion inside a building.
         IEEE Transactions on Geoscience and Remote Sensing, **47**,
         5 (May 2009), 1297–1300.

[21]   Masbernat, X. P., et al.
         An MIMO-MTI approach for through-the-wall radar
         imaging applications.
         In *Proceedings of the 5th International Waveform Diversity
         & Design Conference*, Niagara Falls, Canada, Aug. 2010,
         pp. 188–192.

[22]   Ralston, T. S., Charvat, G. L., and Peabody, J. E.
         Real-time through-wall imaging using an ultrawideband
         multiple-input multiple-output (MIMO) phased array
         radar system.
         In *Proceedings of the IEEE International Symposium on
         Phased Array Systems and Technology*, Waltham, MA, Oct.
         2010, pp. 551–558.

[23]   Ender, J. H. G. and Klare, J.
         System architectures and algorithms for radar imaging by
         MIMO-SAR.
         In *Proceedings of the IEEE Radar Conference*, Pasadena,
         CA, May 2009.

[24]   Li, J. and Stoica, P. (Eds.)
         MIMO Radar Signal Processing.
         Hoboken, NJ: Wiley, 2008.

[25]   Hoctor, R. T. and Kassam, S. A.
         The unifying role of the coarray in aperture synthesis for
         coherent and incoherent imaging.
         Proceedings of the IEEE, **78**, 4 (Apr. 1990), 735–752.

[26]   Ahmad, F., et al.
         Design and implementation of near-field, wideband
         synthetic aperture beamformers.
         IEEE Transactions on Aerospace and Electronic Systems,
         40, 1 (Jan. 2004), 206–220.

[27]   Ahmad, F. and Kassam, S. A.
         Coarray analysis of the wide-band point spread function
         for active array imaging.
         Signal Processing, **81**, 1 (Jan. 2001), 99–115.

[28]   Sévigny, P., et al.
         Concept of operation and preliminary experimental results
         of the DRDC through-wall SAR system.
         Proceedings of the SPIE—Radar Sensor Technology XIV,
         7669 (Apr. 2010), pp. 766907-1–766907-11.

[29]   Deng, H.
         Polyphase code design for orthogonal netted radar
         systems.
         IEEE Transactions on Signal Processing, **52**, 11 (Nov.
         2004), 3126–3135.

[30]   Khan, H. A., et al.
         Optimizing polyphase sequences for orthogonal netted
         radar.
         IEEE Signal Processing Letters, **13**, 10 (Oct. 2006),
         589–592.

[31]   Chen, C-Y. and Vaidyanathan, P.
         MIMO radar ambiguity properties and optimization using
         frequency-hopping waveforms.
         IEEE Transactions on Signal Processing, **56**, 12 (Dec.
         2008), 5926–5936.

[32]   He, H., Stoica, P., and Li, J.
         Designing unimodular sequence sets with good
         correlations—Including an application to MIMO radar.
         IEEE Transactions on Signal Processing, **57**, 11 (Nov.
         2009), 4391–4405.

[33]   Ahmad, F., Zhang, Y., and Amin, M. G.
         Three-dimensional wideband beamforming for imaging
         through a single wall.
         IEEE Geoscience and Remote Sensing Letters, **5**, 2 (Apr.
         2008), 176–179.

[34]   Ahmad, F., Amin, M. G., and Kassam, S. A.
         Synthetic aperture beamformer for imaging through a
         dielectric wall.
         IEEE Transactions on Aerospace and Electronic Systems,
         41, 1 (Jan. 2005), 271–283.

Moeness Amin (F'01) received his Ph.D. degree in 1984 from University of Colorado, in electrical engineering. He has been a member of the faculty of the Department of Electrical and Computer Engineering at Villanova University since 1985. In 2002, he became the Director of the Center for Advanced Communications, College of Engineering. Dr. Amin is the recipient of the 2009 Individual Technical Achievement Award from the European Association of Signal Processing, and the recipient of the 2010 NATO Scientific Achievement Award. He is a Fellow of the International Society of Optical Engineering, and a Fellow of the Institute of Engineering and Technology (IET). He is a recipient of the IEEE Third Millennium Medal, recipient of the Chief of Naval Research Challenge Award, 2010, Distinguished Lecturer of the IEEE Signal Processing Society, 2003 to 2004, active member of the Franklin Institute Committee on Science and the Arts, recipient of Villanova University Outstanding Faculty Research Award, 1997, and the recipient of the IEEE Philadelphia Section Award, 1997. He is a member of SPIE, EURASIP, ION, Eta Kappa Nu, Sigma Xi, and Phi Kappa Phi.

He has over 450 journal and conference publications in the areas of wireless communications, time-frequency analysis, smart antennas, waveform design and diversity, interference cancellation in broadband communication platforms, anti-jam GPS, target localization and tracking, direction finding, channel diversity and equalization, ultrasound imaging and radar signal processing. He is a recipient of seven best paper awards. Dr. Amin currently serves on the Overview Board of the *IEEE Transactions on Signal Processing*. He also serves on the Editorial Board of the *EURASIP Journal on Advances in Signal Processing* and the Editorial Board of the *Signal Processing Magazine*. He was a plenary speaker at ICASSP 2010. Dr. Amin was the Special Session Cochair of the 2008 IEEE International Conference on Acoustics, Speech, and Signal Processing. He was the Technical Program Chair of the 2nd IEEE International Symposium on Signal Processing and Information Technology, 2002. Dr. Amin was the General and Organization Chair of the IEEE Workshop on Statistical Signal and Array Processing, 2000. He was the General and Organization Chair of the IEEE International Symposium on Time-Frequency and Time-Scale Analysis, 1994. He was an Associate Editor of the *IEEE Transactions on Signal Processing* during 1996–1998. He was a member of the IEEE Signal Processing Society Technical Committee on Signal Processing for Communications during 1998–2002. He was a member of the IEEE Signal Processing Society Technical Committee on Statistical Signal and Array Processing during 1995–1997.

Dr. Amin was the Guest Editor of the *Journal of Franklin Institute* September 2008 Special Issue on Advances in Indoor Radar Imaging. He was a Guest Editor of the *IEEE Transactions on Geoscience and Remote Sensing* May 2009 Special Issue on Remote Sensing of Building Interior, and a Guest Editor of the *IET Signal Processing* December 2009 Special Issue on Time-Frequency Approach to Radar Detection, Imaging, and Classification.
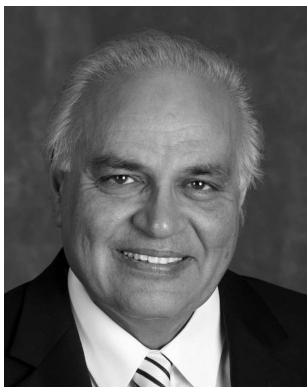
Fauzia Ahmad (S'97—M'97—SM'06) received her M.S. degree in electrical engineering in 1996 and Ph.D. degree in electrical engineering in 1997, both from the University of Pennsylvania, Philadelphia. From 1998 to 2000, she was an assistant professor in the College of Electrical and Mechanical Engineering, National University of Sciences and Technology, Pakistan. During 2000 to 2001, she served as an assistant professor at Fizaia College of Information Technology, Pakistan. Since 2002, she has been with the Center for Advanced Communications, Villanova University, where she is now a research associate professor and the Director of the Radar Imaging Lab.

Dr. Ahmad has over 120 journal and conference publications in the areas of radar imaging, radar signal processing, waveform design and diversity, compressive sensing, array signal processing, sensor networks, ultrasound imaging, and over-the-horizon radar.